Research Square

Preprints are preliminary reports that have not undergone peer review.
They should not be considered conclusive, used to inform clinical practice,
or referenced by the media as validated information.

Black & Bright Auroral Vortices - Driven by Mirrored Rolling Magnetic Carpets

XIAOYAN ZHOU

xyzhou@epss.ucla.edu

University of California, Los Angeles

Donald Hampton

University of Alaska Fairbanks

Christopher Chaston

University of California

Daniel Costanzo

University of California, Los Angeles

Article

Keywords:

Posted Date: September 21st, 2026

DOI: https://doi.org/10.21203/rs.3.rs-11001598/v1

License: This work is licensed under a Creative Commons Attribution 4.0 International License.
Read Full License

Additional Declarations: There is **NO** Competing Interest.

Black & Bright Auroral Vortices
- Driven by Mirrored Rolling Magnetic Carpets

Xiaoyan Zhou[1], Donald Hampton[2], Christopher Chaston[3], and Daniel Costanzo[1]

[1]Department of Earth, Planetary and Space Sciences, University of California, Los Angeles, California, USA
[2]Geophysical Institute, University of Alaska, Fairbanks, USA
[3]Space Sciences Laboratory, University of California, Berkeley, CA, USA

Auroral emissions occur mainly when electrons streaming downward along geomagnetic field lines collide with the upper atmosphere at high latitudes, appearing in two types: diffuse and discrete. Diffuse aurora is faint and patchy, resulting from electron wave scattering. Discrete auroras (e.g., arcs, vortices, omega bands, etc.) are due to electron precipitation along geomagnetic field-aligned currents. However, the field-aligned current generation and circuit configuration of auroral vortices remain unknown. Here, we show a mechanism of rolling magnetic carpets, initiated by azimuthal flow shears in the near-tail plasma sheet. We found that a Kelvin-Helmholtz vortex in the inner plasma sheet (6-8 Earth radii) could roll up magnetic fields, like coiling up a carpet (while generating field-aligned currents). It bridges vortices in the ionosphere and those in the magnetotail, producing a black/bright spiraling auroral footprint when it carries field-aligned current into/away from the ionosphere. At the equator, the circuit is initiated and sustained by a generator $\boldsymbol{j \cdot E < 0}$. Whereas in the ionosphere, the circuit has a load of $\boldsymbol{j \cdot E > 0}$. We have demonstrated that tracing auroral vortices outward can effectively identify field-aligned current generation in remote regions, which can extend to the broader correlation between auroral dynamics and shear flows in the outer magnetosphere.

Investigations of auroral vortices have continued since the pioneering observational and theoretical studies by Davis and Hallinan in 1976 [1,2]. Observations revealed that an auroral vortex could occur singly, in a pair, or as a street stretching more than 600 km, crossing an all-sky image from west to east. The vortices have dimensions ranging from 20 to several hundred km and evolve over a few minutes[1,3-6]. Vortices in any medium indicate shear. In most cases, shear flows collocate with vortices, such as whirlpools in the ocean and Kelvin-Helmholtz (KH) clouds in the atmosphere. Uniquely, the plasma shears associated with auroral vortices are ex situ, remotely located in the magnetosphere. This is because auroral vortices are discrete auroral structures generated by precipitating energetic electrons along the magnetic field from the magnetosphere. Therefore, the remote plasma shear flows hold the key to the formation of auroral vortices.

Most theories suggested that auroral vortices formed from the pre-existing upward field-aligned current (FAC) sheet (as the one during the substorm growth phase) when the sheet broke up into segments[5] or was distorted in the magnetosphere, turning into ripples or spirals due to perturbations[2,3]. A linear analysis using ideal MHD[7,8] showed that a hybrid vortex could be formed in the equatorial plane of the tail plasma sheet due to Rayleigh-Taylor instability coupled with the KH instability, which may have contributed to the intensification of the auroral arc at substorm breakup. However, those theories did not provide energy sources for electron precipitation and lack a mechanism for current closure. Here, we address these two key issues and present a new scenario of the auroral vortex street formation. We find that FACs are generated at the equatorial KH vortex due to the flow vorticity and the self-consistent action of the Lorentz force, complying with $j \cdot E < 0$. These currents are then dissipated in the ionosphere with $j \cdot E > 0$.

A global view of mirrored rolling magnetic carpets

A rolling magnetic carpet[6] is a physicalized messenger that conveys the configuration of an equatorial KH vortex and its energy information to both ionospheres simultaneously. Figure 1a illustrates a pair of rolling magnetic carpets, mirroring each other, and the two associated systems: the bright auroral vortex-related system on the right and the black auroral system on the left. Both occur around magnetic midnight but are viewed from the side to better present the 3-D perspective of the rolling carpet. The KH vortex rolls up the magnetic flux, much like coiling a carpet, creating a spiral rather than a closed circle at its ionospheric footprint. The right and left rolling magnetic carpets mirror each other's configurations, carrying FACs in opposite directions. As a result, there is a bright/black auroral vortex on the right/left. The bottom center shows KH vortex streets in plasma density ratio along the Y direction in the inner tail plasma sheet. The 3-D fluid-kinetic simulations[9] suggest that fast-convection channels in the magnetosphere are unstable, leading to KH instability and KH vortex streets.

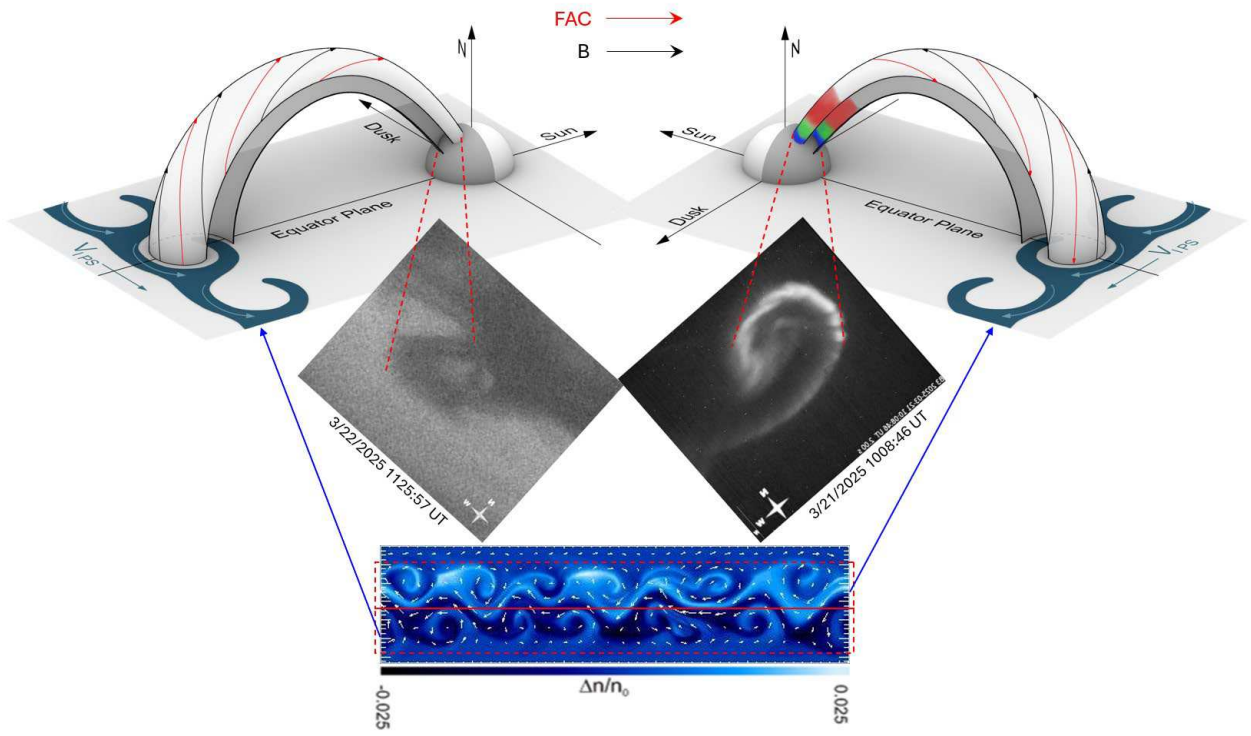

Figure 1a. Reversed auroral vortices and their driving systems. The auroral vortices are oriented as viewed from space along the geomagnetic field. The bright and black auroral vortices are in the ionosphere, the mirrored rolling magnetic carpets in the near-midnight meridian, and the KH vortex streets on the inner tail equator. The red-green-blue ribbon at the ionospheric footprint of the right rolling carpet mimics aurora emissions excited by precipitating electrons along the upward FACs (see more discussion for Figure 3). The bottom center shows a simulation result of KH vortices in two rows in an enhanced version of Fig. 3e in Chaston[9], with overlapped flow vectors in white. The longest vector corresponds to a flow speed of 96 km/s. The top KH vortex street has polarity and flow direction consistent with those (in dark green) at the equatorial end of the rolling magnetic carpet on the right. The bottom KH vortex street is consistent with those on the left. The auroral vortex streets are shown in Figure 2.

Figure 1b illustrates the expansion of 1a to the southern hemisphere and the completion of circuits. During KH vortex development, both flow vorticity ($\nabla \times V$) and the magnetic component of the Lorentz force ($j \times B$) play key roles in FAC generation and closure. The vorticity-related FAC is typically axial and located at the center of the vortical magnetic flux tube[10-11]. The current density

is proportional to the integration along the magnetic field line and the integrated azimuthal B_φ (due to the vorticity) along the radius of the rolling magnetic flux, i.e., $j_{\parallel V} \propto \int_0^h dz \int_0^R B_\varphi dr$ (the subscript V represents vorticity)[10]. At the equator, the Lorentz force ($j_\perp B_{IPS}$) acts against the transferred mechanical stress at the KH vortex, where the most intense magnetic shear stress occurs. It propagates in the Alfvén mode along the internal field. A field-aligned sheet arises from the divergence of $j_\perp$, leading to $j_{\parallel L} \propto \frac{\rho_{IPS} V_{IPS}^2}{B_{IPS}}$ (where subscripts L for Lorentz force, IPS for inner plasma sheet, and V_{IPS} is along the Y axis)[12]. In the next section, we provide an estimate of the ionospheric $j_{\parallel L}$ and compare it with the current density calculated from the auroral vortices imaging data.

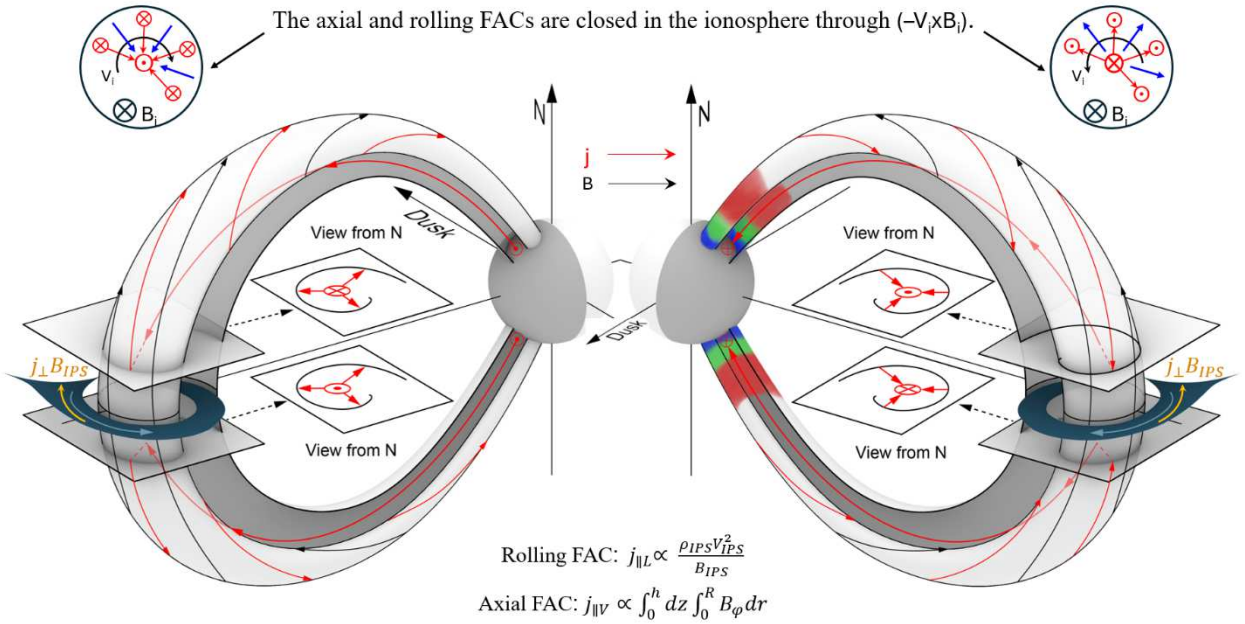

Figure 1b. The global view of the mirrored rolling magnetic carpet with the corresponding circuits and the aurora hemispheric conjugacy. Square planes intersecting the rolling carpet are added to show the FACs' closure hidden within the rolling flux. On each shifted-out plane, the spiral curve is the cutting trace of the rolling magnetic carpet; red arrows are $j_\perp$; small circles with a dot or a cross show the axial FAC (i.e., $j_{\parallel V}$) direction, which is reversed due to

96 the flip of the B_φ direction across the equator. As the Lorentz force acts against shear stress, $j_\perp B_{IPS}$ should be in the
97 opposite direction to the flow along with the KH vortex, resulting in inward/outward $j_\perp$, corresponding to the
98 duskward/dawnward azimuthal flow. In the ionosphere, the axial FAC and rolling FACs are closed via the current
99 along $E = -V_i \times B_i$, as shown on the two circles at the top.

100

101 To depict the FAC directions and their closure, we add intersecting planes above and below the
102 equator. At the equator, the magnetic field lines are bent in the azimuthal direction by the azimuthal
103 flow, resulting in opposite B_φ across the equator and therefore reversing the axial FACs. As the
104 Lorentz force acts against the shear stress/flow, $j_\perp B_{IPS}$ is in the opposite direction to the flow at
105 the equatorial KH vortex. As such, $j_\perp$ must point inward from the rolling carpet sheet to the flux
106 center on the right, i.e., the FACs on the rolling current sheet connect to the axial FAC through the
107 inward-pointing $j_\perp$ (as shown on the displaced intersecting plane), whether they are right above or
108 below the equator. Consequently, the circuits in the northern and southern hemispheres are
109 separated, with FACs out from the ionosphere on the rolling magnetic carpet and into the
110 ionosphere at the center of the flux (see the right section of Figure 1b). This is consistent with the
111 bright auroral vortex in the ionosphere that has an illuminated spiral arm and a dark spot at its
112 center in Figure 1a. Its conjugate aurora in the south will be a bright vortex marking the footprint
113 of the rolling magnetic carpet in the southern ionosphere. Such current systems are also consistent
114 with the reversed FAC circuits between the north and south in Fig. 2 of Chaston[9]. When the
115 equatorial flow direction reverses, so do the Lorentz force and $j_\perp$. The outward $j_\perp$ closes the axial
116 and rolling FACs as shown on the left in Figure 1b. The axial FAC is away from the ionosphere,
117 sending electrons downward and exciting an auroral spot, while the rolling FACs on the carpet
118 sheet are toward the ionosphere and form a black vortex after pulling electrons away from its
119 ionospheric footprint, as shown by the black auroral vortex image in Figure 1a.

In the ionosphere, the downward axial FAC and upward FACs on the rolling carpet sheet is closed via the current $j_{\perp i}$ along $E = -V_i \times B_i$ (the blue arrows in the circles at the two top corners in Figure 1b). Here, red indicates currents, B_i denotes the Earth's magnetic field in the ionosphere, and V_i is the ionospheric flow. In the southern ionosphere, the circuits are symmetric to those in the north. Therefore, bright/black auroral vortices occur on the right/left with FACs flowing out/into the southern ionosphere.

Bright and black Auroral vortices and their FAC density

The two auroral vortex events in Figure 1 were observed from Poker Flat Research Range, AK, on two consecutive days using the same cameras and settings described in Zhou and Hampton[6]. The black and white all-sky images shown in Figure 2 are green emission at 557.7 nm (except for the middle-far-right one). The bright auroral vortices in the top two rows started at ~10 UT on March 21, 2025, and lasted ~20 min. The far-right image on the second row is the Meinel (0-0) auroral vortex at ~1100 nm recorded by the NIR InGaAs camera of the BALBOA balloon project[13], which has the FOV of 62°(H)x51°(V), looking at the trapezoidal area in the image above it. By pointing to the magnetic zenith, the NIR image provided a zoomed-in view of the vortex, showing delicate structures around the magnetic zenith (the red 100 x 100-pixel square).

In general, black aurora (or void aurora) was found to be shear-related when it occurred at the conjunction of diffuse and discrete aurora[14-15]. The black vortices on March 22, 2025 (in the bottom row) appeared and developed in such conjunction with the diffuse aurora in the south and the discrete aurora in the north. They grew out from a black auroral "arc" from east to west across the

sky. Two black spots rolled out from ~11:24:57 UT, but only one vortex was maintained by 11:25:35 UT. This vortex contained a faint auroral spot at its center, as seen in the two images at 11:25:49 and 11:25:57 UT. The vortex dimensions estimated using the NIR image (not shown here) are ~55 x 33 km (east-west by north-south) at 100 km altitude. The formation of black auroral vortex can be explained by the rolling magnetic carpet on the left in Figure 1.

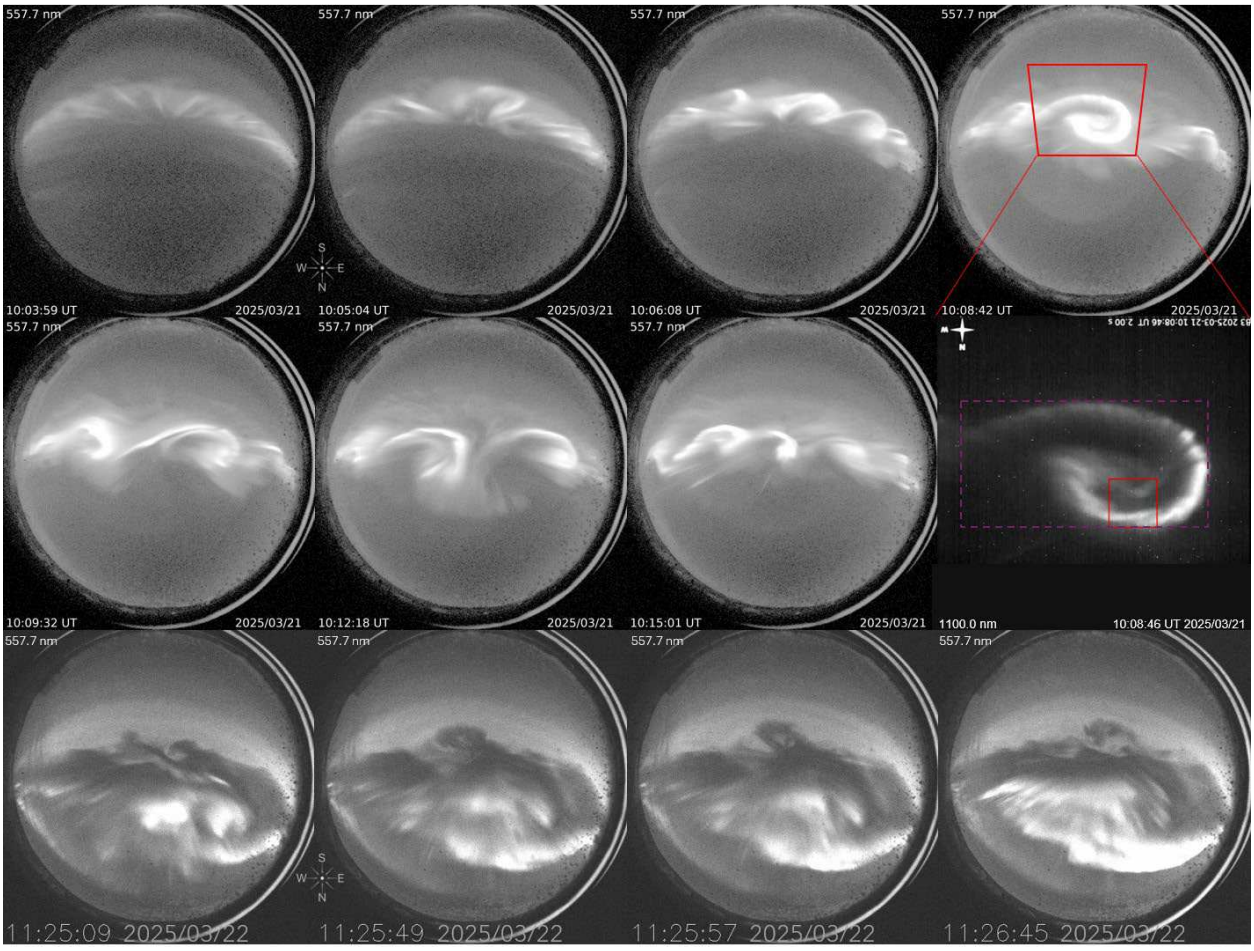

Figure 2. The evolution of the bright and black auroral vortices referred to in Figure 1. In each image, north is at the bottom, and west is to the left. All images are of the green auroral emission at 557.7 nm, except for the right image in the second row, which shows the Meinel aurora at ~1100 nm. The rectangle marked by the purple dashed line indicates the bright vortex dimensions of 91 x 47 km (east-west x north-south at 100 km altitude). Movies of the two auroral

vortex events are available in the Supplementary Information and show the vortices' initiation, evolution, and dynamics.

We recorded the auroral vortices during both events at four wavelengths: 427.8, 557.7, 630.0, and 1100 nm. If we align the bright vortex at ~10:08:40 UT on March 21, 2025, based on the corresponding altitudes of each emission, a colorful cylindrical auroral vortex would have stretched ~200 km in height, as shown in Figure 3. The red emission, corresponding to O(1D), was caused by soft electrons with a few hundred eV. Energetic electrons up to several keV penetrated to lower altitudes. They excited the green emission of O(1S), the blue of N2+(1N), and the invisible NIR N2+ Meinel (0-0) band (see more explanations about the altitude profile dependence in Supplementary Information). Figure 3 provides a zoomed-in 3-D view of the ionospheric footprint of the rolling magnetic carpet, which appears as a colorful cylinder (simplified from the spiraling cylinder as shown by the color ribbon in Figure 1) around 10:08:40 UT (2:08 am AKT).

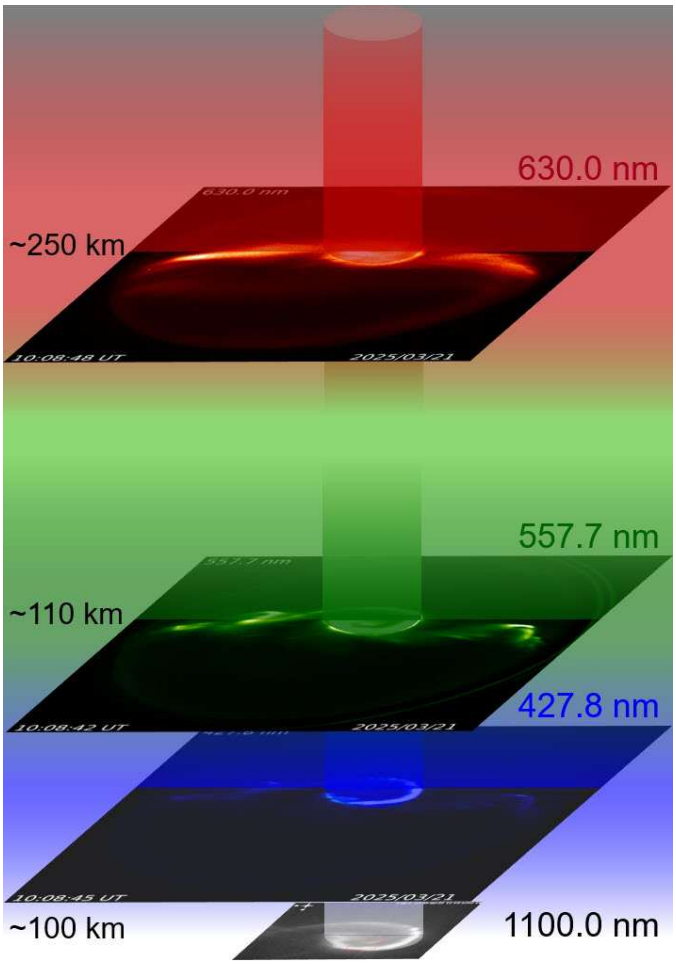

Figure 3. The bright auroral vortex cylinder, ~200 km high, at ~10:08:40 UT on March 21, 2025. The red image was taken at 10:08:48 UT, the green at 10:08:42 UT, and the blue at 10:08:45 UT, using three narrow-bandpass filters on the DASC (digital all-sky camera) filter wheel. The invisible Meinel (0-0) auroral image was at 10:08:46 UT.

Table 1. Auroral vortices in numbers

Date	Time (UT)	E_{avg} (keV)	E_{flux} (mW/m^2)	$j_{\parallel}$ ($\mu A/m^2$)	Size (km) (EWxNS)	Substorm expansion
1/1/2024	~10:19 UT	4-6	30-40	5-10	30x40 (bright spiral)	Y
3/21/2025	~10:08 UT	8-10	40-50	4-6	90x47 (bright spiral)	N
3/22/2025	~11:26 UT	0.8-1.0	1.5	1.5-2.0	17x12 (bright core)*	N
3/22/2025	~11:26 UT	2-3	2.5	N/A	Diffuse background**	N/A

* The size of the black spiral is ~55 x 33 km (EWxNS). ** A diffuse area north of and adjacent to the black spiral.

Observations at multiple wavelengths, both at and around the magnetic zenith, allowed us to calculate the average energy and energy flux of precipitating electrons. This method was discussed and applied in Zhou and Hampton[6]. Table 1 presents the results from three auroral vortex events, including the field-aligned current density estimated using $j_{\parallel} = E_{flux}/E_{avg}$ (a first-order estimation for a monoenergetic distribution). We were extra cautious when analyzing and calculating E_{avg} and E_{flux} responsible for the bright core at the center of the black spiral. The details are in the Supplementary Information.

As the aurora is the rolling magnetic carpet footprint, this aurora-derived $j_{\parallel}$ should be consistent with the FAC density in the ionosphere ($j_{\parallel,ion}$) on the rolling magnetic carpet, which is initiated by the Lorentz force at the flow shears in the inner tail plasma sheet, as discussed in the previous section. We calculated $j_{\parallel,ion}$ using the formula below.

$$J_{\parallel,ion} = \varepsilon \sqrt{\frac{B_{ion}}{B_{IPS}}} \cdot \frac{\rho_{IPS} V_{IPS}^2}{B_{IPS}} \quad (1)$$

Where $\varepsilon = \frac{\alpha l_{\parallel}}{S_b}$, subscripts *ion* and *IPS* refer to the ionosphere and the inner plasma sheet. This formula is the same as equation (3) in Zhou et al.[12], derived from the balance equation between the mechanical momentum of the shear flow and the Lorentz force acting against the transferred mechanical stress at the magnetopause. Here we replaced the values at the dawn flank of the magnetopause with those in the inner plasma sheet with $N_{IPS} = 1.0\ cm^{-3}$, $B_{IPS} = 35\ nT$ in the Z direction of GSM, $V_{IPS} = 200\ km/s$ in the Y direction, and $B_{ion} = 0.54\ G$, then we obtained $J_{\parallel,ion} = \varepsilon \cdot 0.075\ A/m$. Using the same value of $\varepsilon = \frac{\alpha l_{\parallel}}{S_b} = 0.1$ as in Zhou et al.[12] and an auroral

spiral arm thickness of 1.0 km, the Lorentz force related $j_{\parallel,ion}$ was found to be 7.5 $\mu A/m^2$. This value is consistent with the field-aligned current density estimated from the auroral imaging data as listed in Table 1 and is also qualitatively in agreement with an equatorial FAC $j_{\parallel} \approx 0.01\ \mu A/m^2$ at L=8-9, after considering a converging factor of 100 from the inner tail equator to the ionosphere. In addition, previous rocket measurements of upward FAC density through a large auroral spiral was $\sim 5\ \mu A/m^2$[16].

Discussions and conclusions

Auroral vortices are the ionospheric footprints of rolling magnetic carpets carrying FACs, which are coiled up by equatorial KH vortex streets along the inner edge of the tail plasma sheet. FACs are initiated and sustained by the enhanced vorticity and self-consistent action of the Lorentz force at KH vortices, complying with $j \cdot E < 0$ because $j_{\perp IPS}$ is in the opposite direction of the electric field $-V_{IPS} \times B_{IPS}$. This indicates that the mechanical work of the Lorentz force against the shear stress converts kinetic energy into electromagnetic energy, constituting a Poynting flux into the auroral ionosphere. Just above it, parallel electric fields provide $J_{\parallel} \cdot E_{\parallel} > 0$ (such as Polar satellite observations[17]), where the electromagnetic energy is transformed into electron kinetic energy to power the auroras we observe. Finally, closure currents, $j_{\perp i}$, deep within the ionosphere itself align with $-V_i \times B_i$ to provide a load with $j \cdot E > 0$ that consumes remnant electromagnetic energy via Joule heating.

The azimuthally distorted geomagnetic field at the equator reverses the axial FACs in opposite directions above and below it, forming mirrored circuits separately in the northern and southern

hemispheres. Consequently, the auroral vortex is hemispheric conjugate, manifesting the two footprints of the rolling magnetic carpet rooted in both ionospheres.

This paper has demonstrated that auroral outward tracing can provide quantitative insights into the structures and dynamics of the outer magnetosphere, thanks to the auroral four-dimensional information: two horizontal spatial dimensions (east-west and north-south), a third dimension of height/color (which allows for inferences about electron energy), and a fourth temporal dimension indicating the dynamics of auroral motion and expansion. For auroral vortices, this information revealed the otherwise invisible messenger – the rolling magnetic carpet, which is supported by theoretical estimates and simulations. As such, we have illustrated how the auroral vortex itself indicated its formation process.

References

1. Davis, T., & Hallinan, T. Auroral spirals, 1. Observations. *Journal of Geophysical Research*, **81**(22), 3953–3958. https://doi.org/10.1029/ja081i022p03953, (1976).
2. Hallinan, T. Auroral spirals, 2. Theory. *Journal of Geophysical Research*, **81**(22), 3959–3965. https://doi.org/10.1029/ja081i022p03959, (1976).
3. Partamies, N., Freeman, M., & Kauristie, K. On the winding of auroral spirals: Interhemispheric observations and Hallinan's theory revisited. *Journal of Geophysical Research*, **106**(A12), 28913–28924. https://doi.org/10.1029/2001ja900093 (2001).
4. Keiling, A., Angelopoulos, V., Weygand, J., Amm, O., Spanswick, E., Donovan, E., et al. Themis ground-space observations during the development of auroral spirals. *Annales Geophysicae*, *27*(11), 4317–4332. https://doi.org/10.5194/angeo-27-4317-2009 (2009).
5. Haerendel, G., & Partamies, N. On the formation of auroral spirals. *Journal of Geophysical Research: Space Physics,* **129**, e2024JA032413. https://doi.org/10.1029/2024JA032413 (2024).
6. Zhou, X.-Y., and Hampton, D. The auroral vortex and rolling magnetic carpet. *Geophysical Research Letters*, **52**, e2025GL114714 https://doi.org/10.1029/2025GL114714 (2025).
7. Voronkov, I., Rankin, R., Frycz, P., Tikhonchuk, V. T., & Samson, J. C. Coupling of shear flow and pressure gradient instabilities. *Journal of Geophysical Research*, **102**(A5), 9639–9650. https://doi.org/10.1029/97ja00386 (1997).
8. Voronkov, I., Samson, J. C., Friedrich, E., Rankin, R., Tikhonchuk, V. T., & Donovan, E. F. On the distinction between, and the relevance of, auroral breakup and substorm expansive phase onset. ISBN: 92-9092-772-0. In *The proceedings of the fifth international conference on substorms, ESA SP-443* (p. 249). (2000).
9. Chaston, C. C. Flow channels and the generation of Alfvénic turbulence along storm-time inner magnetospheric field-lines. *Geophysical Research Letters*, **49**, e2022GL101321. https://doi.org/10.1029/2022GL101321 (2022).
10. Song, Y., and Lysak, R. L. Displacement current and the generation of parallel electric fields. *Phys. Rev. Lett.* **96**, doi:10.1103/physrevlett.145002-4 (2006).
11. Birn, J., Borovsky, J. E., Hesse, M., & Kepko, L. Substorm current wedge: Energy conversion and current diversion. *Journal of Geophysical Research: Space Physics*, **125**, e2020JA028073. https://doi.org/10.1029/2020JA028073 (2020).
12. Zhou, X.-Y., Haerendel, G., Moen, J. I., Trondsen, E., Clausen, L., Strangeway, R. J., et al. Shock aurora: Field-aligned discrete structures moving along the dawnside oval. *Journal of Geophysical Research: Space Physics*, **122(3)**, 3145–3162. https://doi.org/10.1002/2016JA022666 (2017).
13. Zhou, X.-Y., Rafol, S. B., Michell, R., Hampton, D., Geach, C., Berk, A., et al. Balloons in the Earth's auroral science—BALBOA's modern exploration. *Journal of Geophysical Research: Space Physics*, **125**(10), e2019JA027603. https://doi.org/10.1029/2019JA027603 (2020).
14. Royrvik, O., Pulsating aurora: Local and global morphology, Ph.D. thesis, Univ. of Alaska, Fairbanks, (1976).
15. Davis, T. N., Observed microstructure of auroral forms, *J. Geomagn. Geoelectr.,* **30***,* 371-380, (1978).

16. Kintner, P.M., and L. J. Cahill, Jr., Current system in an auroral substorm, *J. Geophys. Res.,* **79**, 4326-4330, (1974).
17. Mozer, F. S., and A. Hull, Origin and geometry of upward parallel electric fields in the auroral acceleration region, *J. Geophys. Res.*, 106(A4), 5763–5778, doi:10.1029/2000JA900117 (2001).

Acknowledgments
This research was supported by NASA Grant 80NSSC18K0937. Xiaoyan Zhou thanks the BALBOA balloon project team, the staff of Poker Flat Research Range (PFRR), and UCLA colleagues for constructive discussions. Work by Christopher Chaston was supported by National Science Foundation (NSF) Award No. 2411605. The PFRR all-sky camera operations are funded through an NSF cooperative agreement, AGS-1840962, to SRI International, with a subcontract to UAF. Donald Hampton was funded through this and NASA Grant 80NSSC18K0937.

Author contributions
Xiaoyan Zhou developed the concept of mirroring rolling magnetic carpet and led the writing of the paper; Donald Hampton analyzed the PFRR auroral imaging data and calculated the precipitating electron average energy and energy flux; Christopher Chaston provided 3-D fluid-kinetic simulations of the Kelvin-Helmholtz vortex streets in the inner tail plasma sheet; Daniel Costanzo conducted NIR imaging data processing and analysis. All authors discussed the analyses and results and commented on the manuscript.

Competing interests
The authors declare no competing interests.

Additional information
Supplementary information the online version contains supplementary material is available for this paper at …

Corresponding author: Xiaoyan Zhou at xyzhou@epss.ucla.edu
Correspondence and requests for materials should be addressed to Xiaoyan Zhou.

Data availability: Auroral data are available at https://optics.gi.alaska.edu/optics/archive/

Supplementary Files

This is a list of supplementary files associated with this preprint. Click to download.

- DescriptionofSI.pdf
- SupplementaryMovie1.mp4
- SupplementaryMovie2.mp4
- SupplementaryInfo.pdf